HHS Public Access

Author manuscript

Sci Transl Med. Author manuscript; available in PMC 2016 May 05.

Published in final edited form as:

Sci Transl Med. 2015 December 23; 7(319): 319ra207. doi:10.1126/scitranslmed.aad2899.

Pacemaker-Induced Transient Asynchrony Suppresses Heart Failure Progression

Jonathan A. Kirk[1,†,#], **Khalid Chakir**[1,†], **Kyoung Hwan Lee**[2,†], **Edward Karst**[3], **Ronald J. Holewinski**[4], **Gianluigi Pironti**[5], **Richard S. Tunin**[1], **Iraklis Pozios**[1], **Theodore P. Abraham**[1], **Pieter de Tombe**[6], **Howard A. Rockman**[5], **Jennifer E. Van Eyk**[1,4], **Roger Craig**[2], **Taraneh G. Farazi**[3], and **David A. Kass**[1,*]

[1]Department of Medicine, Johns Hopkins University School of Medicine, Baltimore, MD, 21205, USA

[2]Department of Cell and Developmental Biology, University of Massachusetts Medical School, Worcester, MA, 01655, USA

[3]St. Jude Medical, Sunnyvale, CA 94085, USA

[4]Advanced Clinical Biosystems Research Institute, Heart Institute and Department of Medicine, Cedars-Sinai Medical Center, Los Angeles, 90048, USA

[5]Department of Medicine, Duke University School of Medicine, Durham, NC, 27710, USA

[6]Department of Cell and Molecular Physiology, Loyola University Stritch School of Medicine, Maywood, IL, 60153, USA

Abstract

Uncoordinated contraction from electromechanical delay worsens heart failure pathophysiology and prognosis, but restoring coordination with bi-ventricular pacing, known as cardiac resynchronization therapy (CRT) improves both. Not every patient, however, qualifies for CRT. Here we show that heart failure with synchronous contraction is improved by inducing dyssynchrony for 6 hours daily by right-ventricular pacing using an intracardiac pacing device, in a process we call pacemaker-induced transient asynchrony (PITA). In dogs with heart failure induced by 6 weeks of atrial tachypacing, PITA (starting on week 3) suppressed progressive

[*]Corresponding Author: dkass@jhmi.edu.
[†]Equal Contributions
[#]Current Affiliation: Department of Cell and Molecular Physiology, Loyola University Stritch School of Medicine, Maywood, IL 60153, USA

Author Contributions: J.A.K. performed skinned myofilament studies, isolated myofibril studies, Western blots, data analysis, prepared manuscript, and provided intellectual input. K.C. performed isolated myocyte functional studies and Western blots. K.H.L. and R.C. conducted electron microscopy and image analysis. E.K. and T.G.F. developed the custom pacemaker software. R.J.H. and J.E.V. conducted mass spectrometry studies. G.P. and H.A.R. conducted β-AR experiments. R.S.T. performed canine surgeries. I.P. and T.P.A. conducted echocardiographic studies. P.dT supervised isolated myofibril studies. D.A.K. orchestrated the study, assisted in data analysis, edited the manuscript, and provided intellectual input.

Competing Interests: J.A.K. and D.A.K. are listed as inventors on a pending patent on the use of temporary dyssynchrony to improve cardiac function in failing hearts. H.A.R. is a scientific cofounder for Trevena Inc., a company that is developing GPCR-targeted drugs. E.K. and T.G.F. hold stock in St. Jude Medical, Inc., which developed the pacemaker system and software.

Data and materials availability: Proteomic data were uploaded to PeptideAtlas (www.peptideatlas.org), accession number: PASS0076.

cardiac dilation as well as chamber and myocyte dysfunction. PITA enhanced β-adrenergic responsiveness in vivo and normalized it in myocytes. Myofilament calcium response declined in dogs with synchronous heart failure, which was accompanied by sarcomere disarray and generation of myofibers with severely reduced function, and these changes were absent in PITA-treated hearts. The benefits of PITA were not replicated when the same number of RV-paced beats was randomly distributed throughout the day, indicating that continuity of dyssynchrony exposure is necessary to trigger the beneficial biological response upon resynchronization. These results suggest PITA could bring the benefits of CRT to the many heart failure patients with synchronous contraction that are not CRT candidates.

Introduction

Congestive heart failure affects tens of millions of patients worldwide and remains a leading cause of hospitalization and death (1). In approximately 20% of patients, the disease is worsened by uncoordinated contraction owing to delays in regional electrical activation (2). This major co-morbidity can be treated by cardiac resynchronization therapy (CRT), which electrically stimulates both sides of the heart's left ventricle to restore coordinate contraction, improving both HF pathophysiology and prognosis in humans (3). These salubrious effects were first attributed to enhanced chamber mechano-energetics, as CRT reduces wasted cardiac work while augmenting systemic blood flow (4). However, studies have since shown CRT also profoundly alters myocardial cell and molecular biology to enhance cell survival (5), myofilament function (6), mitochondrial energetics (7), ion channel regulation (8), and beta-adrenergic receptor signaling (9, 10). Intriguingly, these changes appear to be a consequence of restoring synchrony in a dyssynchronous failing heart, rather than being a generalized response to hemodynamic improvement (5–8).

In HF patients with dyssynchrony, CRT enhances function and outcomes beyond that observed in failing human hearts that were never dyssynchronous (3). This suggests the process of transitioning from dyssynchrony to synchrony may itself confer molecular/cellular benefits. If so, then one might also improve synchronous HF by purposely inducing dyssynchrony for a limited period of time, and then reversing it. We first explored this concept in dogs; surprisingly, rather than worsening the outcome, a two-week mid-sequence exposure to dyssynchrony (atrial pacing followed by dyssynchronous, returning to atrial) improved β-adrenergic and myofibrillar function (6, 9) over HF hearts that were never dyssynchronous. This concept of transiently exposing an organ to a stimulus that could be damaging if sustained, with the goal of gaining benefits upon their removal, is also common in neuro-stimulation and immune therapies. In this instance, the therapy is not the stimulus itself, but the host's reactive biology that ensues after its removal.

Applying dyssynchrony for one or more weeks has limitations, because the effective duty cycle – in other words, how long one waits before repeating exposure – can vary individually, and prolonging exposure to dyssynchrony and thus reduced function may not be well tolerated. To circumvent this, we investigated daily exposure to a period of dyssynchrony followed by resynchronization, which we have termed pacemaker induced transient asynchrony (PITA), in dogs with synchronous heart failure from chronic rapid-

atrial pacing. We then compared PITA biological and physiological outcomes to HF dogs that received only atrial-tachypacing and to healthy control animals. Compared to synchronous HF, PITA attenuated progressive chamber dilation and maladaptive remodeling, augmented β-adrenergic responsiveness at chamber and myocyte levels, and yielded normal myofiber structure, contractile function, and cellular force generation.

RESULTS

PITA blunts progressive chamber dilation and improves β-adrenergic response in HF

Dogs with synchronous HF from chronic rapid-atrial pacing (11) received pacemaker induced transient asynchrony (PITA), consisting of right ventricular rapid-pacing (dyssynchrony) from 00:00–06:00 each day and atrial rapid-pacing (synchrony) for the remaining 18 hours. PITA was initiated after two weeks of 100% atrial tachypacing to pre-establish HF. At the end of the six-week protocol, PITA was compared to both HF controls that received only atrial tachypacing throughout and healthy controls. Both PITA and HF dogs were paced at the same rapid rate (200 min^{-1}), with the only variable being which lead was used, while control dogs were unpaced. We subjected PITA dogs to nighttime dyssynchrony because this is when they are least active. Both HF and PITA dogs were monitored for 24-hour periods to confirm continuous pacing-capture, and in PITA dogs, ventricular pacing occurred from 00:00 to 06:00 with atrial pacing the rest of the day (fig. S1).

Figure 1A shows example 2-D echocardiograms for HF and PITA-treated hearts at initial baseline and six weeks (end of study), demonstrating smaller end-diastolic volume with PITA treatment. Summary data for left ventricular volume (ESV, end-systolic volume) and ejection fraction (EF) (Fig. 1, B and C), and corresponding end-diastolic pressure (EDP) (Fig. 1D) reveal significant increases in ESV and EDP and decreases in EF after two weeks of atrial tachypacing. By six weeks, both HF and PITA-treated dogs had dilated further, but dilation was less marked with PITA therapy (Fig. 1, A and B). Similarly, EF declined 2-fold and EDP increased 4-fold in HF animals as compared to baseline values, and both EF and EDP changes were partially ameliorated by PITA (Fig. 1, C and D). Although PITA introduced dyssynchrony each night, there was no apparent “memory effect” once atrial pacing was restored during the day. The normal synchronous heart has a dyssynchrony index of 26.9 ± 2.6 versus 75 with dyssynchrony (10). Both HF and PITA models displayed normal synchrony during daytime atrial pacing (HF = 22.5 ± 1.7, PITA = 22.4 ± 3.5).

Intact heart β-adrenergic receptor (β-AR) responsiveness was measured by exposure to intravenous dobutamine. Figure 1E shows example pressure tracings before and after maximal dobutamine stimulation. PITA treatment enhanced maximal rates of pressure rise and decline compared with HF (fig. S2). At baseline, $dP/dt_{max}/IP$ (maximal rate of pressure rise normalized to simultaneous pressure, a contractility index with less load sensitivity) similarly declined in both HF and PITA groups compared to healthy controls (Fig. 1F). However, PITA-treated hearts displayed an enhanced dobutamine dose-response compared to HF dogs at all doses, resulting in a 38% relative increase in the maximum dobutamine response at 15 mcg/kg/min. At this maximum dose, systolic function in PITA-treated hearts was similar to healthy controls, whereas it remained depressed in HF dogs.

PITA enhances myocyte β-adrenergic responsiveness and receptor density

In cardiac myocytes from dogs with HF, baseline sarcomere shortening was depressed compared to both healthy control cells and cells from PITA-treated hearts (Fig. 2A). Corresponding disparities were observed in peak calcium transients (Fig. 2A). HF myocytes also displayed a blunted β-adrenergic response to non-selective (isoproterenol) and selective (β1-receptor, norepinephrine + prazosin) stimulation. However, cells from PITA-treated hearts displayed essentially normal responses with both forms of beta-adrenergic stimulation (Fig. 2A). Although we did not measure isolated myocyte behavior in a separate group of dogs at the 2-week (pre-PITA) time point, prior studies report substantial beta-adrenergic down-regulation occurs by 1-week of tachypacing (12). Thus, these normal responses with PITA suggest functional improvement after initiation of treatment, rather than inhibition of deterioration.

CRT globally upregulates β2-AR responsiveness by blunting inhibitory G-protein ($G\alpha_i$) coupling—a change linked to enhanced expression of regulators of G-protein signaling, RGS2 and RGS3 (9). We tested if this mechanism applies to PITA by exposing myocytes to a selective β2-AR agonist, zinterol, with or without pre-treatment with the $G\alpha_i$ inhibitor, pertussis toxin. Unlike CRT, β2-AR–stimulated sarcomere shortening remained depressed after PITA and in HF, and pertussis toxin increased this zinterol response similarly in both groups (fig. S3), indicating the β2-AR response contributed very little to the overall β-adrenergic response observed with isoproterenol stimulation in the myocyte and dobutamine stimulation *in vivo*. RGS3 and $G\alpha_i$ protein expression rose similarly in both groups, whereas RGS2 and $G\alpha_s$ were not significantly different from healthy controls (fig. S4). Thus, mechanisms for PITA-related β-AR responsiveness differed from those previously identified from CRT (9, 10).

Isoproterenol-stimulated cyclic AMP declined in HF myocytes versus controls, and PITA enhanced this response (Fig. 2B). Cells exposed to the direct adenylyl cyclase activator forskolin showed a similar response pattern (Fig. 2B), but differences were relatively small as compared to β-adrenergic receptor stimulation. Collectively, these data suggest PITA modulates membrane receptor density more than G-protein coupling or cyclase activity. This hypothesis was tested by a radiolabeled ligand binding assay which revealed that both β1 and β2 adrenergic membrane receptor density were reduced in HF and higher with PITA (Fig. 2C). This change in receptor density was not transcriptionally regulated, as mRNA expression was similar for both receptors (fig. S5A). As receptor density may decline from phosphorylation by G protein-coupled receptor kinases GRK2 or GRK5, we assessed protein expression of each. Both rose similarly in HF and PITA groups (fig. S5B), and so unlikely explained the disparity.

PITA-treated myocytes have normal myofilament calcium activation

Systolic reserve also depends on the myofilament response to calcium, which is globally depressed in both synchronous and dyssynchronous HF and normalized by CRT (6). To test the impact of PITA on this behavior, myocytes were isolated from the left ventricle (lateral wall endocardium), chemically skinned and then exposed to steady-state calcium. Maximal activated force (F_{max}) normalized to cellular cross sectional area declined in HF and was

fully restored by PITA (Fig. 3A). However, cross sectional area had increased in HF myocytes (Fig. 3, B to D) and this change principally explained the decline in normalized F_{max}, as peak force alone was similar among the three groups (Fig. 3E).

HF also shifted the force-calcium relationship leftward (calcium sensitization or decline in EC_{50}) (Fig. 3A), which PITA reversed. The sensitization with HF was consistent with reduced troponin I (TnI) phosphorylation at S22/S23 (13) (Fig. 3F) and a rise in GSK-3β activity (6) reflected by a decline in its phosphorylation at S9 (Fig. 3G**).** Reduced TnI S22/S23 phosphorylation was also observed with PITA, but GSK-3β-S9 was more phosphorylated (reducing activity), which desensitizes myofilaments. This reduced GSK-3β activity and calcium desensitization with PITA is consistent with changes observed with dyssynchrony (6).

PITA improves sarcomere structure and myofiber depression with HF

Unaltered maximal force despite greater cell cross-sectional area with HF suggests the presence of either a sub-population of very weakened myofibrils or a widespread moderate weakening of all myofibrils, which are normalized in PITA treated hearts. We therefore examined skinned myocytes by electron microscopy. Many sarcomeres from HF cells exhibited structural defects (Fig. 4A), including a wider and wavier Z-band along with wavy/misaligned actin-myosin filaments (Fig. 4B, arrows). Transverse sections showed more space between myofibrils and a reduced myofibril diameter, an appearance also seen in longitudinal sections (Fig. 4C). In control myofibrils, a regular hexagonal arrangement of myosin filaments each surrounded by six symmetrically placed actin filaments was observed and confirmed by Fourier analysis (Fig. 4C, inset). In many HF myofibrils, this arrangement was less ordered, with a more diffuse FFT. PITA treated cells displayed a normal myofibrillar structural pattern, fiber size, and inter-myofibrillar space, although a wider, wavier Z-band remained. In both Control and PITA cells there was normal sarcomere structure, whereas in HF, among 3,727 imaged sarcomeres, 1,525 (40%) had disarrayed myofilaments (Fig. 4D). These disarrayed sarcomeres clustered in regions, with <20% of imaged fields exhibiting both normal and disarrayed sarcomeres (Fig. 4E).

To test if heterogeneity of sarcomere structure reflected functional disparities in sub-populations of myofibrils, myocytes were disrupted and maximum force in individual myofibrils assessed. Similar to whole, chemically skinned myocytes, mean myofibrillar F_{max} declined in HF but was normal with PITA (Fig. 4F). However, this was not due to a general population behavior, but rather to the presence of a sub-group of very low-force generating fibrils in HF (7/18 of those tested, ~40%), defined by F_{max}<150% of noise levels (dashed line, Fig. 4F). Only one such myofibril (out of 18) was found in PITA-treated hearts and none (out of 15) in healthy controls. By excluding low-force generating myofibrils, we noted similar myofibrillar F_{max} among the groups (Fig. 4G).

To test if disrupted myofibrils in HF resulted from deficiencies in myofilament protein expression, we performed non-biased quantitative proteomics using SWATH-MS to determine protein concentrations from myofilament-enriched samples. There were 490 unambiguous proteins quantified (table S1). Proteins involved with motor force generation, such as troponin I (TnI), troponin T (TnT), troponin C (TnC), tropomyosin (Tm), actin,

obscurin, titin, α-actinin, myosin binding protein C (MyBPC), and myosin light chains (MLC1, MLC2), were similarly expressed in each group (Fig. 5A). Four proteins showed differential expression (one-way ANOVA, false discovery rate/$q<0.05$, $p<0.0017$); of these, two differed between HF and PITA (Holm-Sidak post-hoc test): Bcl2-associated athanogene 3 (BAG3) and nebulin-related anchoring protein (NRAP). Both BAG3 and NRAP increased with HF, but rather than reversing with PITA, they increased even more (Fig. 5B), indicating these proteins, involved in forming and maintaining sarcomere structure, may be elements of a compensatory mechanism.

Randomly distributed dyssynchrony does not replicate benefits from PITA

A key concept underlying PITA is that dyssynchrony is applied for a contiguous period of time sufficient to induce biological effects that lead to benefits following resynchronization. In this key sense, the therapy should not be equivalent to random dyssynchrony such as occurs in patients who develop frequent premature ventricular contractions or lose CRT pacing in a dyssynchronous failing heart, both thought to worsen disease (14–16). To test this, we altered the pacemaker program to flip a 4-sided coin every 2 minutes, with RV pacing instituted only if one specific side was obtained. Thus, the RV was paced for 25% of the day, similar to PITA, but this was distributed randomly, as confirmed by 24-hour monitoring (fig. S6). The random protocol was initiated at week 3 (Rand) in 6 dogs and week 1 (Rand6) in 3 dogs.

In contrast to PITA, *in vivo* cardiac function was unaltered over HF in hearts receiving randomly distributed RV pacing (Fig. 6, A and B). Intravenous dobutamine induced similar augmentation of dP/dt_{max}/IP in both groups (Fig. 6C). Isolated myocytes also showed similar reduced rest and isoproterenol-stimulated contraction and peak calcium transient responses (Fig. 6D). Sarcomere function, as measured by F_{max}, and calcium sensitivity, EC_{50}, was unchanged in myocytes from the dogs receiving random pacing initiated at the beginning of the protocol compared to those from HF dogs (Fig. 6E). Further, cells from randomly paced hearts displayed similar myofilament disarray as in HF (Fig. 6, F and G), where 22.5% of 3067 sarcomeres displayed the disarrayed phenotype observed in HF. Thus, randomly inducing dyssynchrony by RV pacing throughout the day did not replicate the benefits from PITA.

Discussion

In this study we show that PITA, a daily circumscribed period of pacemaker-induced cardiac dyssynchrony that is then reversed, suppresses progressive heart dilation, and enhances *in vivo* and cellular beta-adrenergic response, intact myocyte function, calcium handling, and myofilament function and ultrastructure in a canine model of tachycardia-induced heart failure. While PITA diminished global dilation and dysfunction it did not prevent it entirely; however, this is not surprising given that tachypacing stress was applied throughout. By comparison with a tachypaced CRT model, PITA reduced chamber volumes even more (5, 10). Myocyte functional improvements from PITA were similar to those reported from CRT in dogs (6, 9), but we found their molecular mechanisms differ, in that PITA did not involve

RGS proteins and had opposing affects on GSK-3β activity, revealing PITA as a new and distinct form of HF therapy.

PITA may at first seem counterintuitive, because dyssynchrony depresses function when sustained, yet here we find benefits when it is applied for several hours daily and then removed. One analogy is myocardial pre-conditioning, where cardiac protection is generated after first applying several brief periods of intense ischemia followed by reperfusion (17). More sustained or randomly induced ischemia depresses function. Interestingly, very short-term dyssynchrony pacing (three 5-minute episodes separated by synchronous pacing) may also induce preconditioning, as reported in a rabbit model (18–20); however, unlike PITA, short-term dyssynchrony would not applicable to chronic human disease.

PITA affected two primary behaviors underlying systolic reserve, β-AR responsiveness and myofilament function, thus blocking defects that otherwise develop with synchronous HF. The primary cause of improved β-AR responsiveness was increased receptor-density, and although several possible explanations were tested, the mechanism remains unclear. The change in calcium sensitivity with PITA is opposite to that from CRT (6), and this difference could relate to disparities in GSK-3β phosphorylation, which declines in synchronous HF and CRT, but increases in dyssynchronous HF (6). The rise in GSK-3β phosphorylation with PITA is consistent with effects from its associated dyssynchrony, and may explain its restoration of calcium sensitivity to normal.

The more prominent change with PITA was recovery of maximal activated force normalized to cell cross sectional area. With HF, this decline in F_{max} was primarily due to a lack of increase in force despite myocyte enlargement—which has been previously observed in experimental and human HF (21–24). Therapies that reduce cell size, such as ventricular assist devices (21), CRT (6, 25), and now PITA, also leave absolute F_{max} unaltered but the normalized value rises. To our knowledge, the data presented here are the first to test if uncoupling of F_{max} and cell size results from generalized myofibrillar depression or the presence of a sub-population of weak myofibrils. Our results support the latter, with a remarkable quantitative similarity in the decline in normalized F_{max} (38%), and the amount of disrupted sarcomeres (40.3%) and weak myofibrils (39%). We cannot prove that the functionally defective myofibrils had damaged sarcomeres, because EM cannot be performed on an isolated myofibril. However, the clustering of structural defects in the EM analysis supports their presence within a given fiber.

The mechanism by which PITA prevents myofibrillar defects remains unanswered. Overall global chamber dilation and stress were less in PITA-treated hearts compared with HF, and this might impact signaling and/or force to stimulate myofibrillogenesis and enhance fiber quality control. Compromised energy availability and reduced protein turnover in HF have been linked to depressed proteasome function and autophagy (26, 27). This might hinder the cell's ability to eliminate poorly formed proteins and structures, compromising sarcomere architecture and function. In this regard, the relative PITA-induced increase of BAG3 and NRAP is intriguing as both are critically involved with sarcomere structure,. BAG3 maintains myofibrillar integrity during mechanical stress via its interaction with heat shock cognate 70 (28), whereas NRAP acts as a scaffold for actin–α-actinin assembly at the start

of myofibrillogenesis (29). That both rose in HF may reflect a compensatory yet inadequate response if cell size is increasing, yet when cells are again smaller as with PITA, their further rise might prove more effective in sarcomere restructuring. Proof of their role cannot be established in the current dog model, but will require development of a chronic pacing mouse model combined with genetic manipulation.

The application of dyssynchronous pacing by PITA differs importantly from conditions where the heart is prematurely activated by abnormal excitable tissue (e.g. extra-systoles) or where CRT is employed in dyssynchronous HF yet intermittently fails to capture both ventricles. Both are considered as contributors to worsening human HF (15, 16). However, dyssynchrony from these clinical settings is not sustained for hours and absent otherwise, but rather randomly distributed throughout the day. We found random dyssynchrony did not replicate PITA benefits, indicating that continuity of dyssynchrony exposure at least long enough to trigger a biological response once it is resynchronized is key to its efficacy. How long this period needs to be and whether there is a better time of day to deliver it than at night, remains to be determined. These are difficult questions to answer in a large animal model given the expense and number of animals required, but may be tested in rodents. The simplicity of the concept suggests one might translate this to humans directly, conducting a proof of concept study first before assessing alternative dosing options.

Our study has some limitations. First, we employed a tachypacing model to induce HF. Although tachycardia is not a very common cause of the disease in humans, it is a well-established and accepted large animal HF model reproducing many organ and cellular/molecular aspects of the human disease (30). Unlike myocardial infarction, which itself leads to uncoordinated wall motion and regional heterogeneity of cellular properties, the current model allowed us to test the effect of a single change: the chamber being paced. Global dilation without regional infarction is a common HF presentation, so the results certainly have implications to a substantial population even if excluding this sub-group. Tachypacing also leads to early global dysfunction (31), and depression of excitation-contraction coupling (32) and β-AR signaling (12), all within days to one week, which is was why we waited until week three to initiate PITA. Our 2-week global data mirror these prior studies, but we did not elect to replicate earlier myocyte findings, as this would require sacrifice of an entirely separate set of dogs at the earlier time point.

We also focused our cellular and molecular analysis to a single site (lateral wall) rather than duplicate these experiments in the anterior wall as well. This is because prior studies in always dyssynchronous hearts have shown both myofibrillar (6) and β-AR regulatory (10) dysfunction are similar in both territories. This also holds for survival signaling and other factors (3). Because PITA induced dyssynchrony for only 6 (versus 24) hours, regional disparities would be even less likely. Our study design did not test if PITA can rescue more advanced HF. Doing so would have required extending the pacing protocol for several months, raising mortality and necessitating a different protocol. However, we did delay implementation until demonstrable disease had been induced. Lastly, canine model do not permit molecular cause-effect analyses.

In summary, transient exposure to dyssynchrony by PITA therapy ameliorates HF pathobiology and improves cardiac rest and reserve function. We identified a novel mechanism for the decrease in maximal activated force in heart failure—the addition of structurally and functionally incompetent myofibers and sarcomeres—and showed that PITA reverses and/or avoids this defect, improving cellular and global function in the process. These results suggest a new therapy for the sizable proportion of HF patients who are not presently candidates for CRT, many of whom already receive implantable programmable stimulation devices to prevent sudden cardiac death or to provide rate-responsive pacing.

Materials and Methods

Study design

The study was designed to identify differences in dogs that were synchronously tachypaced for the entire pacing protocol (six weeks) and those that were treated with pacemaker-induced transient asynchrony (PITA). A subgroup of dogs was randomly assigned to the Control group and received no pacing. The HF and PITA groups were paced at the right atria 100% for the first two weeks. All paced dogs received echocardiographic and hemodynanmic measurements at baseline (prior to pacing) and at the two-week time point. At the beginning of week 3, dogs were randomly assigned to either continued atrial pacing (HF) or PITA-treatment. At the end of the six-week protocol, echocardiographic, hemodynamic, and dobutamine challenge experiments were conducted. The animal was then euthanized, heart tissue harvested, and additional experiments conducted as described below. The number of dogs in each group was determined by power analysis (for *in vivo* results) and to match our previous work with this dog model of heart failure (5, 6, 9, 10), although *n* values for each assay done on tissue samples varied based on that particular experiment and are indicated in each figure legend.

Canine Models

All studies were approved by the Johns Hopkins Animal Care and Use Committee, and performed by trained personnel. Details of the canine model have been reported previously (5, 10). For the current study, an Anthem CRT-P pacemaker (PM3212, St. Jude Medical) was modified via an MTA between Johns Hopkins University and St. Jude Medical. The proprietary device communicated with a custom laptop-based programmer/emulator and pacemaker firmware to pace at 200 bpm (above the device's normal upper limit of 180), and automatically implement time-of-day changes in pacing mode (RV versus RA). With the exception of healthy controls, animals were tachypaced at 200 bpm, 24 hours per day, in VVI mode for six weeks to induce HF, with one group (HF) being atrially paced the entire time, and the other receiving PITA (atrial pacing from 06:00–24:00, RV pacing from 00:00–06:00) starting on week 3. RV free-wall pacing induces LV dyssynchrony similar to that with a left bundle branch block as indexed by variance in wall motion timing by tissue Doppler (10). Note that, at present, a fully implantable device with the time-of-day switch to alter between synchrony and dyssynchrony pacing has not been commercially developed, but recommended methods for reproducing this program are provided in Supplementary methods.

A third group received RV pacing starting on week 3, but distributed randomly during the 24 hours. The algorithm followed a 4-sided coin flip assigning RV:atrial pacing site at a 1:3 ratio. Lastly, three dogs received random pacing starting on week 1. At the end of study, animals were anesthetized with pentobarbital, intubated, and the heart excised under ice-cold cardioplegia.

Intact myocyte isolation and functional studies

Primary isolated left ventricular myocytes were obtained as previously described (10). Cells from lateral endocardium were studied, as cell function and adrenergic signaling have been shown to be similar from this and anterior/septal walls in the pacing models (10). Sarcomere shortening and whole-cell calcium transients were assessed with an inverted microscope (Ellipse TE2001, Nikon) equipped with an image-fluorescence system (MyoCam, IonOptix). Studies were performed at 37°C, and cells field stimulated at 1 Hz, as described (10). Drug doses were: 100 nM isoproterenol (ISO), 100 nM norepinephrine (NE), 1 μM prazocin (Prz), 1 μM zinterol (Zin), and 1.5 μg/mL pertussus toxin (PTX), as used previously (9, 10).

Isolated Myofibrils

Tissue from the endocardium of the left ventricular lateral wall was flash frozen in liquid nitrogen and stored at −80°C. Isolated myofibril functional experiments were carried out as described (33). Briefly, thin strips of tissue were dissected from the tissue and were "skinned" in relaxing solution plus 1% Triton X-100. Muscle strips were then mechanically homogenized in the presence of relaxing buffer, but without Triton. The myofibrils were lifted between two glass microtools, a very stiff holding probe and an L-shaped force probe. Sarcomere length was calculated from the FFT of the image. Sarcomere length was set at 2.1 μm. The deflection of the force probe in response to contraction of the myofibril was detected by a split photo-diode placed at the camera port of the inverted microscope. The myofibril was maintained at 15°C during this experiment.

Electron microscopy

Membrane-permeabilized myocytes were prepared as described in Supplementary Methods. Isolated cardiac myocytes were fixed with 2.5% glutaraldehyde in 0.1 M phosphate buffer, pH 7.4, at room temperature for 2 hours. Fixed myocytes were post-fixed with 1% OsO_4 in 0.1 M sodium cacodylate buffer, dehydrated in a graded alcohol series, and embedded in Epon. Sections (70 nm thick) were cut with a diamond knife, then stained on copper grids with uranyl acetate followed by lead citrate (34). Images were obtained at 80 kV on a TECNAI Spirit transmission electron microscope (FEI) using a Gatan Erlangshen CCD camera. Fast Fourier transforms of selected regions were obtained using the ImageJ (National Institutes of Health) FFT function (process/FFT/FFT).

β-AR density

Myocardial sarcolemmal membranes were prepared by homogenizing whole hearts in ice cold buffer containing 50 mM Tris, 2 mM EDTA, 12.5 mM $MgCl_2$, 10 mM sucrose, 2 μg/ml Aprotinin, and 2 μg/ml Leupeptin. Membrane protein concentration was determined by the

Bio-Rad protein assay. Total specific binding was determined by incubating the 25 μg of membrane homogenate with a saturating concentration of ^{125}I-cyanopindolol (500 pM, Perkin Elmer) in binding buffer.

Total βAR density was determined using 20 mM alprenolol, while 300 nmol/L of CGP 20712A was used to saturate all β1-ARs. β2-AR density was obtained by subtracting β1-AR density to total β-AR density. Binding assays were conducted at 37°C for 90 min and terminated by rapid vacuum filtration over glass fiber filters (Whatman GF/B catalogue #: FPD-196), which were subsequently washed and counted in a gamma counter. Specific binding was reported as fmol of receptor per mg of membrane protein.

SWATH Mass Spectrometry

Myofilament-enriched samples were solubilized in 8 M urea, 0.1% SDS. For each sample 200 μg of protein was digested using the FASP (35). Samples were digested with a trypsin/Lys-C solution, acidified with TFA and desalted on Oasis HLB μ-elution plates (Waters), eluting with 80% ACN, 0.1% FA and drying down the samples. Samples were resuspended in 0.1% FA at a concentration of 4 μg/μl for LC-MS/MS analysis.

Samples were analyzed on a 5600 TripleTOF mass spectrometer (Sciex) equipped with an Eksigent ekspert 415 nanoLC, Ekspert cHiPLC, and Ekspert nanoLC 400 autosampler. Pooled samples were analyzed in shotgun mode (data dependent acquisition, DDA) to create a spectral ion library. Individual samples were analyzed using data independent acquisition (SWATH) with 100 variable SWATH windows from 400–1250 m/z. For both DDA and SWATH acquisitions (also known as DIA, data independent acquisition), samples were loaded onto a trap column (nano cHiPLC Trap) for 10 minutes and then separated using a nano cHiPLC ChromXP C18-CL column using a linear AB gradient from 5–35% solvent B, where A is composed of 0.1% aqueous FA and B is 0.1% FA in CAN, for 120 min, 35–85% B for 2 minutes, holding at 85% for 5 minutes, then re-equilibration at 5% B for 17 minutes. Exogenous retention time peptide standards (iRT, Biognosys) were spiked in to each sample directly before both DDA and SWATH analysis.

DDA files were searched using the Paragon algorithm[2] using the canine uniprot (July 2014) library, resulting in 529 proteins (this is the library, 490 proteins were unambiguously identified in the individual samples) and 8803 peptides identified at 1% global FDR. The resulting .group file was loaded into the SWATH 2.0 microapp within the PeakView software (Sciex) to construct the peptide ion library. The resulting ion library was uploaded into the BaseSpace OneOmics cloud server (https://basespace.illumina.com/) and protein areas were calculated using the Protein Expression Extractor app within BaseSpace, implementing the most likely ratios normalization. Individual protein areas were then normalized to βMHC protein area for each sample.

Statistical Analyses

Comparisons between multiple experimental groups (with no repeated measures) were performed by one-way ANOVA with Holm-Sidak post-hoc test. Data involving multiple treatments (Fig. 2A, Fig 6D, fig. S2, fig. S3) were analyzed by two-ANOVA with Holm-Sidak post-hoc test. Dobutamine dose data (Fig. 1F) were analyzed by ANACOVA, one-way

ANOVA at each dose, and Holm-Sidak post-hoc test. Myofibril data (Fig. 4F) were analyzed by Mann-Whitney Rank Sum non-parametric test, HF vs. Control and PITA. Prior to analysis, end-diastolic pressure data was transformed using a standard $-\log_{10}$ transformation, as raw data was non-normal. Repeated measures were treated as independent to avoid issues with missing data points. $p < 0.05$ was considered significant.

Supplementary Material

Refer to Web version on PubMed Central for supplementary material.

Acknowledgments

We thank N. Witayavanitkul, A. Dvornikov, and M. Phillip for their technical expertise and assistance.

Funding: This work was supported by the NIH (P01-HL077180 to D.A.K. and J.V.E., T32-HL007227, P01-HL059408, Abraham and Virginia Weiss and Michael and Janet Huff Endowments to D.A.K., NHLBI-HV-10-05(2) to J.V.E., HHSN268201000032C to J.V.E., R01-AR034711 to R.C., and P01-HL75443 to H.A.R.) the American Heart Association (14SDG20380148 to J.A.K.), and the Burroughs Wellcome Fund (1012753 to J.A.K.).

References and notes

1. Mozaffarian D, Benjamin EJ, Go AS, Arnett DK, Blaha MJ, Cushman M, de Ferranti S, Despres JP, Fullerton HJ, Howard VJ, Huffman MD, Judd SE, Kissela BM, Lackland DT, Lichtman JH, Lisabeth LD, Liu S, Mackey RH, Matchar DB, McGuire DK, Mohler ER 3rd, Moy CS, Muntner P, Mussolino ME, Nasir K, Neumar RW, Nichol G, Palaniappan L, Pandey DK, Reeves MJ, Rodriguez CJ, Sorlie PD, Stein J, Towfighi A, Turan TN, Virani SS, Willey JZ, Woo D, Yeh RW, Turner MB. C. American Heart Association Statistics, S. Stroke Statistics. Heart disease and stroke statistics--2015 update: a report from the American Heart Association. Circulation. 2015; 131:e29–322. [PubMed: 25520374]
2. Tracy CM, Epstein AE, Darbar D, Dimarco JP, Dunbar SB, Estes NA 3rd, Ferguson TB Jr, Hammill SC, Karasik PE, Link MS, Marine JE, Schoenfeld MH, Shanker AJ, Silka MJ, Stevenson LW, Stevenson WG, Varosy PD. 2012 ACCF/AHA/HRS focused update of the 2008 guidelines for device-based therapy of cardiac rhythm abnormalities: a report of the American College of Cardiology Foundation/American Heart Association Task Force on Practice Guidelines. Journal of the American College of Cardiology. 2012; 60:1297–1313. [PubMed: 22975230]
3. Kirk JA, Kass DA. Electromechanical dyssynchrony and resynchronization of the failing heart. Circ Res. 2013; 113:765–776. [PubMed: 23989718]
4. Nelson GS, Berger RD, Fetics BJ, Talbot M, Hare JM, Spinelli JC, Kass DA. Left ventricular or biventricular pacing improves cardiac function at diminished energy cost in patients with dilated cardiomyopathy and left bundle-branch block. Circulation. 2000; 102:3053–3059. [PubMed: 11120694]
5. Chakir K, Daya SK, Tunin RS, Helm RH, Byrne MJ, Dimaano VL, Lardo AC, Abraham TP, Tomaselli GF, Kass DA. Reversal of global apoptosis and regional stress kinase activation by cardiac resynchronization. Circulation. 2008; 117:1369–1377. [PubMed: 18316490]
6. Kirk JA, Holewinski RJ, Kooij V, Agnetti G, Tunin RS, Witayavanitkul N, de Tombe PP, Gao WD, Van Eyk J, Kass DA. Cardiac resynchronization sensitizes the sarcomere to calcium by reactivating GSK-3beta. J Clin Invest. 2014; 124:129–138. [PubMed: 24292707]
7. Wang SB, Foster DB, Rucker J, O'Rourke B, Kass DA, Van Eyk JE. Redox regulation of mitochondrial ATP synthase: implications for cardiac resynchronization therapy. Circ Res. 2011; 109:750–757. [PubMed: 21817160]
8. Aiba T, Tomaselli G. Electrical remodeling in dyssynchrony and resynchronization. J Cardiovasc Transl Res. 2012; 5:170–179. [PubMed: 22271011]
9. Chakir K, Depry C, Dimaano VL, Zhu WZ, Vanderheyden M, Bartunek J, Abraham TP, Tomaselli GF, Liu SB, Xiang YK, Zhang M, Takimoto E, Dulin N, Xiao RP, Zhang J, Kass DA. Galphas-

biased beta2-adrenergic receptor signaling from restoring synchronous contraction in the failing heart. Sci Transl Med. 2011; 3:100ra188.

10. Chakir K, Daya SK, Aiba T, Tunin RS, Dimaano VL, Abraham TP, Jaques-Robinson KM, Lai EW, Pacak K, Zhu WZ, Xiao RP, Tomaselli GF, Kass DA. Mechanisms of enhanced beta-adrenergic reserve from cardiac resynchronization therapy. Circulation. 2009; 119:1231–1240. [PubMed: 19237665]
11. Moe GW, Armstrong P. Pacing-induced heart failure: a model to study the mechanism of disease progression and novel therapy in heart failure. Cardiovasc Res. 1999; 42:591–599. [PubMed: 10533598]
12. Kiuchi K, Shannon RP, Komamura K, Cohen DJ, Bianchi C, Homcy CJ, Vatner SF, Vatner DE. Myocardial beta-adrenergic receptor function during the development of pacing-induced heart failure. J Clin Invest. 1993; 91:907–914. [PubMed: 8383704]
13. van der Velden J, Papp Z, Zaremba R, Boontje NM, de Jong JW, Owen VJ, Burton PB, Goldmann P, Jaquet K, Stienen GJ. Increased Ca2+-sensitivity of the contractile apparatus in end-stage human heart failure results from altered phosphorylation of contractile proteins. Cardiovasc Res. 2003; 57:37–47. [PubMed: 12504812]
14. Latchamsetty R, Bogun F. Premature Ventricular Complexes and Premature Ventricular Complex Induced Cardiomyopathy. Current problems in cardiology. 2015; 40:379–422. [PubMed: 26282347]
15. Hayes DL, Boehmer JP, Day JD, Gilliam FR 3rd, Heidenreich PA, Seth M, Jones PW, Saxon LA. Cardiac resynchronization therapy and the relationship of percent biventricular pacing to symptoms and survival. Heart Rhythm. 2011; 8:1469–1475. [PubMed: 21699828]
16. Koplan BA, Kaplan AJ, Weiner S, Jones PW, Seth M, Christman SA. Heart failure decompensation and all-cause mortality in relation to percent biventricular pacing in patients with heart failure: is a goal of 100% biventricular pacing necessary? J Am Coll Cardiol. 2009; 53:355–360. [PubMed: 19161886]
17. Murry CE, Jennings RB, Reimer KA. Preconditioning with ischemia: a delay of lethal cell injury in ischemic myocardium. Circulation. 1986; 74:1124–1136. [PubMed: 3769170]
18. Vanagt WY, Cornelussen RN, Poulina QP, Blaauw E, Vernooy K, Cleutjens JP, van Bilsen M, Delhaas T, Prinzen FW. Pacing-induced dys-synchrony preconditions rabbit myocardium against ischemia/reperfusion injury. Circulation. 2006; 114:I264–I269. [PubMed: 16820583]
19. Vanagt WY, Cornelussen RN, Baynham TC, Van Hunnik A, Poulina QP, Babiker F, Spinelli J, Delhaas T, Prinzen FW. Pacing-induced dyssynchrony during early reperfusion reduces infarct size. J Am Coll Cardiol. 2007; 49:1813–1819. [PubMed: 17466233]
20. Babiker FA, Lorenzen-Schmidt I, Mokelke E, Vanagt WY, Delhaas T, Waltenberger J, Cleutjens JP, Prinzen FW. Long-term protection and mechanism of pacing-induced postconditioning in the heart. Basic Res Cardiol. 2010; 105:523–533. [PubMed: 20336304]
21. Ambardekar AV, Walker JS, Walker LA, Cleveland JC Jr, Lowes BD, Buttrick PM. Incomplete recovery of myocyte contractile function despite improvement of myocardial architecture with left ventricular assist device support. Circ Heart Fail. 2011; 4:425–432. [PubMed: 21540356]
22. Belin RJ, Sumandea MP, Kobayashi T, Walker LA, Rundell VL, Urboniene D, Yuzhakova M, Ruch SH, Geenen DL, Solaro RJ, de Tombe PP. Left ventricular myofilament dysfunction in rat experimental hypertrophy and congestive heart failure. Am J Physiol Heart Circ Physiol. 2006; 291:H2344–2353. [PubMed: 16815982]
23. Fan D, Wannenburg T, de Tombe PP. Decreased myocyte tension development and calcium responsiveness in rat right ventricular pressure overload. Circulation. 1997; 95:2312–2317. [PubMed: 9142010]
24. Bito V, van der Velden J, Claus P, Dommke C, Van Lommel A, Mortelmans L, Verbeken E, Bijnens B, Stienen G, Sipido KR. Reduced force generating capacity in myocytes from chronically ischemic, hibernating myocardium. Circ Res. 2007; 100:229–237. [PubMed: 17234974]
25. Orrego CM, Nasir N, Oliveira GH, Flores-Arredondo JH, Cordero-Reyes AM, Loebe M, Youker KA, Torre-Amione G. Cellular evidence of reverse cardiac remodeling induced by cardiac resynchronization therapy. Congestive heart failure (Greenwich, Conn). 2011; 17:140–146.

26. Gupta A, Akki A, Wang Y, Leppo MK, Chacko VP, Foster DB, Caceres V, Shi S, Kirk JA, Su J, Lai S, Paolocci N, Steenbergen C, Gerstenblith G, Weiss RG. Creatine kinase-mediated improvement of function in failing mouse hearts provides causal evidence the failing heart is energy starved. The Journal of clinical investigation. 2012; 122:291–302. [PubMed: 22201686]
27. Willis MS, Patterson C. Proteotoxicity and cardiac dysfunction--Alzheimer's disease of the heart? N Engl J Med. 2013; 368:455–464. [PubMed: 23363499]
28. Hishiya A, Kitazawa T, Takayama S. BAG3 and Hsc70 interact with actin capping protein CapZ to maintain myofibrillar integrity under mechanical stress. Circ Res. 2010; 107:1220–1231. [PubMed: 20884878]
29. Manisastry SM, Zaal KJ, Horowits R. Myofibril assembly visualized by imaging N-RAP, alpha-actinin, and actin in living cardiomyocytes. Exp Cell Res. 2009; 315:2126–2139. [PubMed: 19233165]
30. Houser SR, Margulies KB, Murphy AM, Spinale FG, Francis GS, Prabhu SD, Rockman HA, Kass DA, Molkentin JD, Sussman MA, Koch WJ. C. o. C. C. American Heart Association Council on Basic Cardiovascular Sciences, G. Council on Functional, B. Translational. Animal models of heart failure: a scientific statement from the American Heart Association. Circ Res. 2012; 111:131–150. [PubMed: 22595296]
31. Komamura K, Shannon RP, Pasipoularides A, Ihara T, Lader AS, Patrick TA, Bishop SP, Vatner SF. Alterations in left ventricular diastolic function in conscious dogs with pacing-induced heart failure. J Clin Invest. 1992; 89:1825–1838. [PubMed: 1601992]
32. Vatner DE, Sato N, Kiuchi K, Shannon RP, Vatner SF. Decrease in myocardial ryanodine receptors and altered excitation-contraction coupling early in the development of heart failure. Circulation. 1994; 90:1423–1430. [PubMed: 7522133]
33. Walker JS, Walker LA, Margulies K, Buttrick P, de Tombe P. Protein kinase A changes calcium sensitivity but not crossbridge kinetics in human cardiac myofibrils. Am J Physiol Heart Circ Physiol. 2011; 301:H138–146. [PubMed: 21498779]
34. Reynolds ES. The use of lead citrate at high pH as an electron-opaque stain in electron microscopy. J Cell Biol. 1963; 17:208–212. [PubMed: 13986422]
35. Wisniewski JR, Zougman A, Nagaraj N, Mann M. Universal sample preparation method for proteome analysis. Nat Methods. 2009; 6:359–362. [PubMed: 19377485]

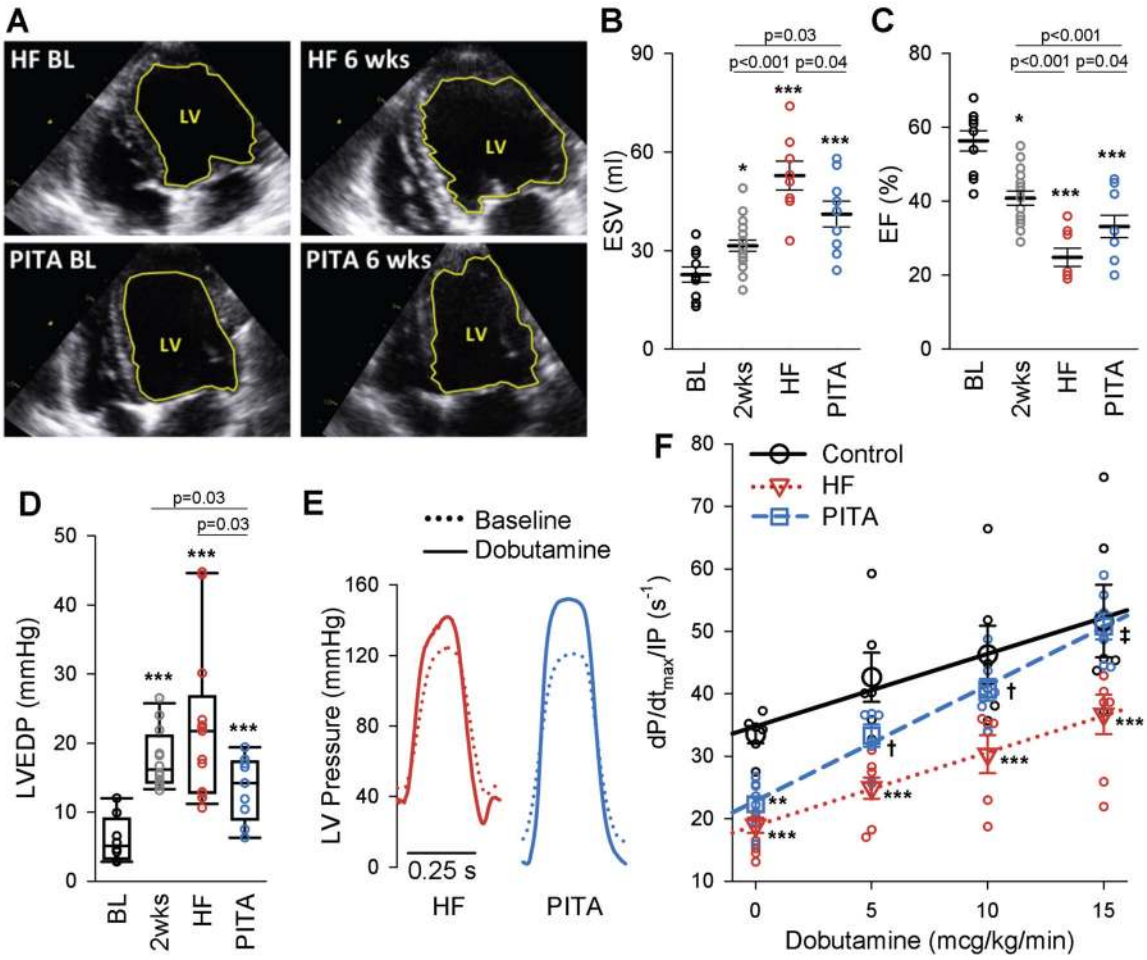

Figure 1. Pacemaker induced transient asynchrony (PITA) improves *in vivo* cardiac function

(**A**) Example end-diastolic echocardiographic images at baseline (BL) and after 6-weeks (end of study) of dog hearts in the heart failure (HF) and PITA treated group. The left-ventricle (LV) is outlined in yellow. (**B** and **C**) LV end-systolic volume (ESV) (B) and ejection fraction (EF) (C) assessed by echocardiography at baseline (BL, $n = 10$), after two weeks of atrial pacing ($n = 18$), at the end of the six-week atrial pacing protocol (HF, $n = 8$), and at the end of six-week PITA protocol ($n = 9$). (**D**) LV end-diastolic pressure (LVEDP) from hemodynamic studies (n: Con = 8, 2wks = 12, HF = 13, PITA = 10 dogs). EDP data were non-normal, and are displayed as box plots. Data were $\log_{10}$-transformed before one-way ANOVA. Direct comparison to 2wks group made by t-test). (**E**) Example LV pressure waveforms in HF and PITA hearts at baseline and with 15 mcg/kg/min dobutamine. (**F**) Dobutamine dose-effect on LV contractility ($dP/dt_{max}/IP$) (n: Control = 6, HF = 9, PITA = 8 dogs, some doses missing for individual dogs). Data points indicate individual animals at each dose, symbols are means ± SEM. *p<0.05, **p<0.01, ***p<0.001 vs. Control; †p<0.05, ‡p<0.001 vs. HF by one-way ANOVA and Holm Sidak post-hoc test.

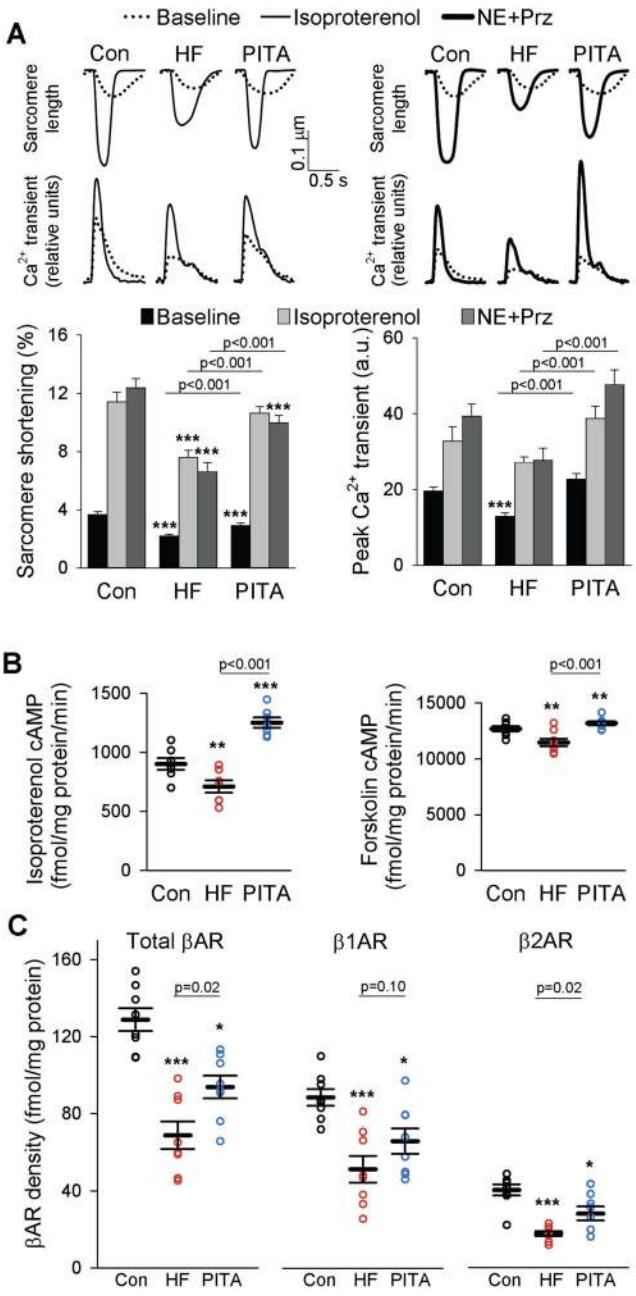

Figure 2. Myocyte function is depressed in HF after β-adrenergic receptor stimulation, but near normal with PITA

(**A**) Example tracings of sarcomere shortening and intracellular calcium transients from LV lateral wall myocytes isolated from healthy control, HF, and PITA dogs at baseline and after isoproterenol stimulation (0.1 μM) or after norepinephrine and prazosin stimulation (NE, 0.1 μM; Prz, 1 μM). Sarcomere shortening and intracellular calcium are quantified below as means ± SEM (n = 4–7 dogs in each group, cells/dog: 5.8 ± 0.4, mean ± SEM). For all three groups, Iso and NE+Prz sarcomere shortening and peak Ca^{2+} transient data are p<0.05 versus respective baseline; ***p<0.001 vs. Control by two-way ANOVA and Holm-Sidak post-hoc test. (**B**) Cyclic AMP activity after isoproterenol or forskolin (FSK) stimulation.

Data are individual dogs ($n = 8$), with means ± S.E.M. (**C**) Plasma membrane β-AR, β1-AR, and β2-AR density. Data are individual dogs and means ± SEM ($n = 8$ per group). In B and C, *p<0.05, **p<0.01, ***p<0.001 vs. Control by one-way ANOVA and Holm-Sidak post-hoc test.

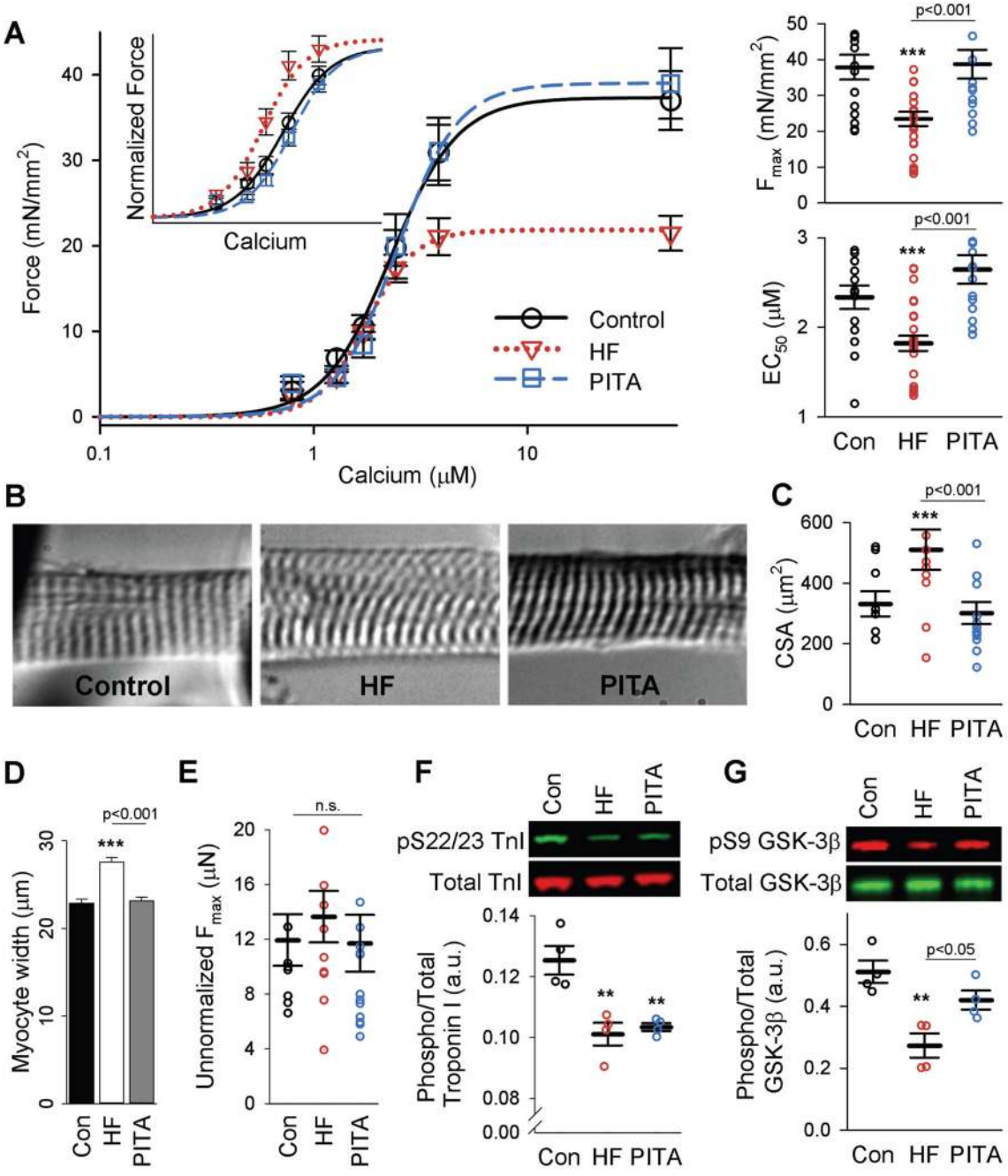

Figure 3. Myofilament function is depressed in HF and recovered with PITA

(**A**) Mean force as a function of calcium concentration (± SEM) and fitted curves for skinned myocytes from the LV lateral wall for Con, HF, and PITA. Inset shows force data normalized to F_{max}. Summary results for F_{max} and EC_{50} from these curve fits are shown as individual myocytes and means ± SEM (*n*: Con = 15 from 6 dogs, HF = 26 myocytes from 8 dogs, PITA = 14 myocytes from 4 dogs, cells/dog = 3 ± 0.2, mean ± SEM). (**B**) Representative images (40x) of Con, HF, and PITA skinned myocytes stretched to a sarcomere length of 2.1 μm. (**C**) Myocyte cross-sectional area (CSA) of all myocytes

examined in A. Data are means ± SEM. (**D**) Mean skinned myocyte width ± SEM (n = 150 cells per group). (**E**) F_{max} from (A) without normalization to CSA. Data are individual myocytes and means ± SEM. (**F**) Phospho-serine 22/23 troponin I (TnI) protein expression normalized to total TnI. Data are individual dogs and means ± SEM (n = 4 per group). (**G**) Phospho-serine 9 GSK-3β normalized to total GSK-3β (n = 4 per group). For all panels, **p<0.01, ***p<0.001 vs. Control, unless otherwise indicated, by one-way ANOVA with Holm-Sidak post-hoc test.

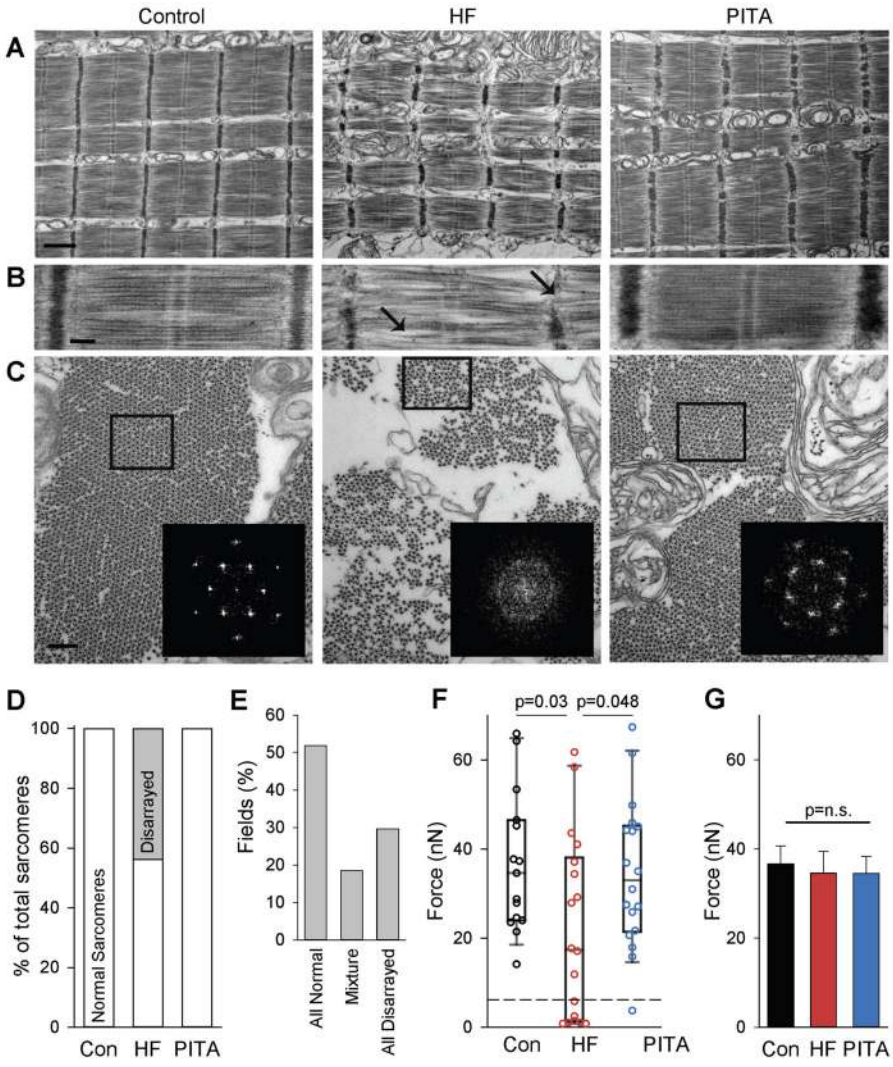

Figure 4. Myofilament structure and function is disrupted in HF, but restored in PITA

(**A**) Longitudinal sections of skinned myocytes imaged by electron microscopy. Normal structures were observed in Control and PITA, but HF sarcomeres showed myofilament disarray. Scale bar, 1 μm. (**B**) Higher magnification highlighting the disrupted myofilament structures: weak and wavy Z-band and M-band, bent/curved filaments with irregular spaces between that were observed in some HF myofibrils, as indicated by arrows. Scale bar, 200 nm. (**C**) Transverse sections of myofilaments, showing smaller diameter of myofibrils with increased space between, and loss of regular filament lattice structure in HF compared with Control and PITA-treated animals. (inset) Fast-Fourier Transforms (FFTs) of boxed areas confirmed loss of normal lattice structure in HF group. Scale bar, 200 nm. (**D**) Percentage of normal and disarrayed sarcomeres identified by electron microscopy ($n = 3727$ sarcomeres examined from $n = 3$ HF dogs). (**E**) Disarrayed sarcomeres cluster together in HF. The percent of EM fields containing normal, disarrayed, or a mixture was quantified in the HF group ($n = 28$ fields). (**F**) Isolated myofibril force. A sub-population of fibrils generating extremely low force is indicated by the dashed line. Data are individual myofibrils and box

plots, as HF data were non-normally distributed (*n*: Con = 15, HF = 18, PITA = 18 myofibrils). *P* values determined by Mann-Whitney Rank Sum non-parametric test. (**G**) F_{max} compared after removing the weak myofibrils from (F) (*n* removed from the analysis: Con = 0, HF = 7, PITA = 1 myofibril). n.s., not significant by one-way ANOVA.

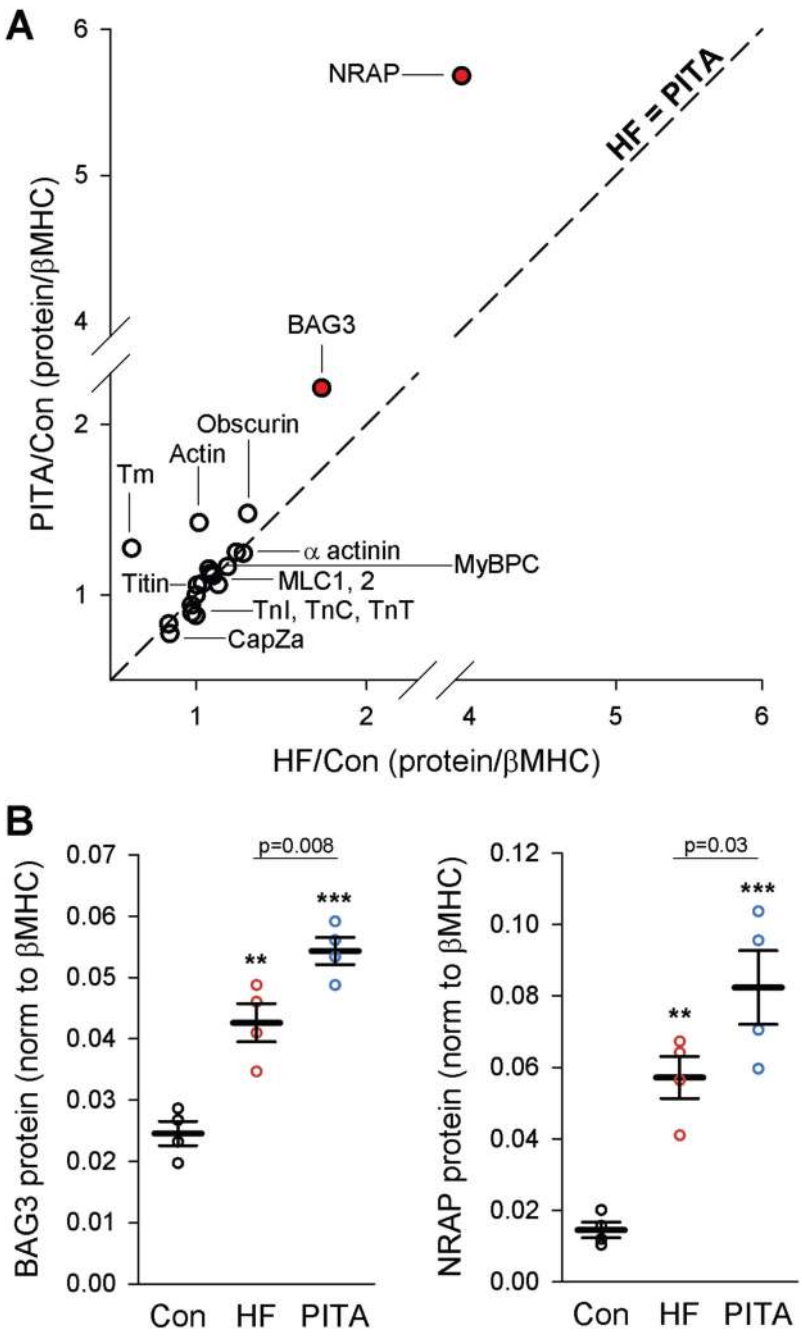

Figure 5. Proteomic analysis of myofilament-enriched samples revealed changes in sarcomere assembly chaperones

(**A**) Ratio of the core myofilament proteins in both HF and PITA normalized to Control samples ($n = 4$). Proteins that lay along the identity line (dashed line, slope = 1) were similarly expressed in HF and PITA. The two red dots (Bcl2-associated athanogene 3, BAG3, and nebulin-related anchoring protein, NRAP) were significantly different between HF and PITA: $p<0.0017$ (false discovery rate = 0.05) by one-way ANOVA. (**B**) SWATH mass spectrometry analysis for BAG3 and NRAP expression. Data are individual animals (n

= 4) and means ± SEM. **p<0.01, ***p<0.001 vs. Control, unless otherwise indicated, by one-way ANOVA and Holm-Sidak post-hoc test.

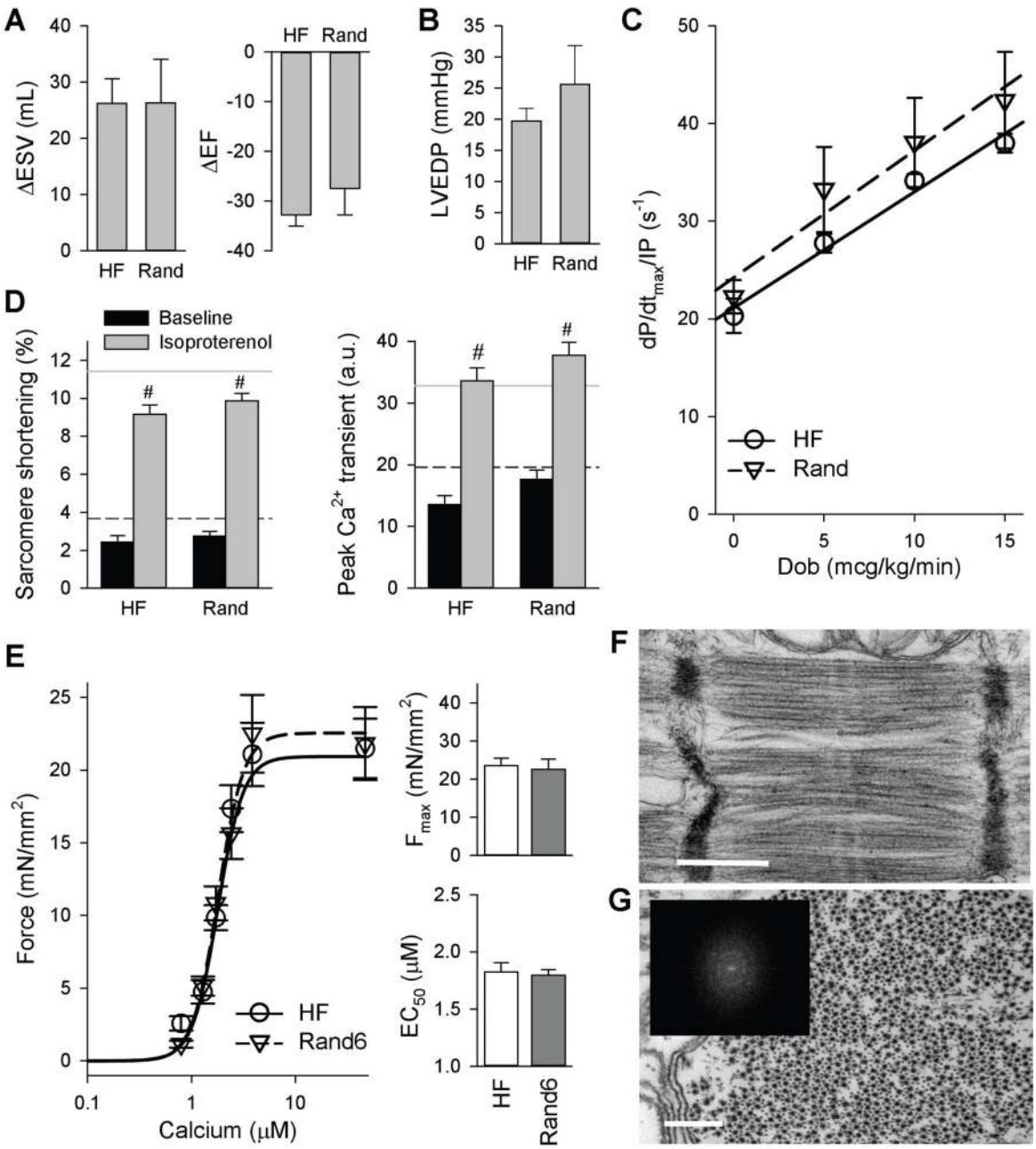

Figure 6. Randomly distributed RV pacing (dyssynchrony) does not confer beneficial effects compared to HF

(**A**) Change in end-systolic volume (ΔESV) and ejection fraction (ΔEF) assessed by serial echocardiography at 6 weeks versus baseline. (**B**) Absolute LVEDP in random RV pacing in HF dogs. (**C**) The influence of dobutamine infusion on contraction ($dP/dt_{max}/IP$). In (A to C), data are means ± SEM (*n*: Rand = 6, HF = 5 dogs). (**D**) Peak sarcomere shortening and peak calcium transient at baseline and with isoproterenol stimulation in HF and Rand. Data are means ± SEM (*n*: Baseline HF: 13 cells from 4 dogs; Baseline Rand: 34 cells from 7 dogs; Iso HF: 30 cells from 4 dogs; Iso Rand: 71 cells from 7 dogs). Black dashed line: baseline control mean, gray line: isoproterenol-stimulated control mean. #p<0.05 vs.

respective baseline by two-way ANOVA and Holm-Sidak post-hoc test. (**E**) Mean force as a function of calcium concentration (± SEM) and fitted curves for myocytes from the LV lateral wall for HF and Rand6 (six weeks of 6 h/day randomly distributed RV pacing). Summary data for F_{max} and calcium sensitivity (EC_{50}) are shown as means ± SEM (*n*: HF = 26 myocytes from 8 dogs, Rand6 = 10 myocytes from 3 dogs). (**F**) EM structural imaging of sarcomeres. Image is representative of $n = 3$. Scale bar, 500 nm. (**G**) Transverse EM image section, showing filament lattice structure. Scale bar, 200 nm. (Inset) FFTs confirmed loss of normal lattice structure.